Periodate as an oxidant for catalytic water oxidation: oxidation via electron transfer or O-atom transfer?

Hetterscheid, D.G.H.; Reek, J.N.H.

EurJIC European Journal of Inorganic Chemistry

ChemPubSoc Europe

FULL PAPER

DOI:10.1002/ejic.201300249

Periodate as an Oxidant for Catalytic Water Oxidation: Oxidation via Electron Transfer or O-Atom Transfer?

CLUSTER ISSUE

Dennis G. H. Hetterscheid*[a,b] and Joost N. H. Reek[b]

Keywords: Water splitting / Homogeneous catalysis / Oxidation / Periodate / Iridium / Density functional calculations

Treatment of **Ir**$(OH)_2$ with sodium periodate in aqueous solution results in formation of dioxygen following the rate law $v = k_{obs}[\mathbf{Ir}]^{0.65}[IO_4]^{0.5}$, with $k_{obs} = 1.5 \times 10^{-3}$ {**Ir**$(OH)_2$ = $[IrCp^*(Me_2NHC)(OH)_2]$, where Me_2NHC = *N*-dimethylimidazolin-2-ylidene and Cp^* = cyclopentadienyl}. In situ ESI-MS experiments in combination with DFT calculations show that $[\mathbf{Ir}^{III}(IO_3)]^+$ and $[\mathbf{Ir}^{V}(=O)(IO_3)]^+$ species are present in the reaction mixture. On the basis of the presence of these species, a mechanistic pathway was calculated illustrating that water is not necessarily the source of the oxygen. A low-lying pathway exists wherein O_2 production proceeds via two consecutive O-atom-transfer reactions from periodate to the catalyst. The resulting iodite ligand is further oxidized to close the catalytic cycle. The rate-determining step in this process is formation of the O–O bond. For this transition a 21.8 kcal/mol barrier was found. This value fits very well with the observed turnover frequency of 0.27 s^{-1}. Although it is difficult to prove that this is the dominant pathway, these data clearly illustrate that one has to be very careful with interpretation of catalytic results in periodate-driven water oxidation reactions.

Introduction

Fossil-fuel reserves are rapidly decreasing and oil reserves in particular will be depleted shortly.[1] Moreover, the total amount of natural gas is limited.[1] Coal is still abundant, but especially since global climate change is directly linked to CO_2 emissions, increased coal usage is undesirable. Hence it is of extreme importance to shift our energy source from fossil fuels to renewable energy. As solar energy is the major source of renewable energy,[2] yet is not abundant for 24 hours a day, it is important that we learn how to store solar energy as a chemical fuel. Water oxidation allows us to split water on irradiation with solar energy and thereby to store solar energy in the form of hydrogen.[2] Consequently, interest in catalytic water oxidation has grown large, and recently various molecular ruthenium,[3] iridium,[4] manganese,[5] iron,[6] cobalt,[7] and even copper catalysts[8] have been reported. Some of these molecular systems have been reported to catalyze more than 20,000 turnovers,[9,4e] and recently a water oxidation system was demonstrated that has a similar rate to the oxygen-evolving center of photosystem II.[10] However, large improvements in catalytic performance and a better general understanding of the mechanisms underlying these catalytic transformations is required to further improve these numbers and allow use of water oxidation catalysts in future industrial applications.

Typically, in a first experiment catalytic water oxidation is tested by addition of a stoichiometric oxidant. Cerium ammonium nitrate (CAN) is most frequently used,[11] despite major drawbacks. The experimental conditions are harsh and the stability of CAN is limited to very acidic conditions (pH < 1), while its oxidation potential is very high (E = 1.8 V vs normal hydrogen electrode).[12] Additionally, CAN may actively take part in the water oxidation process, rather than being an innocent one-electron oxidant. Berlinguette et al. showed that incorporation of O^- from nitrate into molecular oxygen can occur in CAN-promoted catalytic water oxidation.[12a] Moreover Sakai et al. illustrated by means of DFT calculations that $[\{Ce(OH)(NO_3)_5\}]^{2-}$, the hydrolysis product of CAN, is better described as a cerium(III) species with a hydroxy radical coordinated.[13] From here it is not difficult to imagine that instead of electron transfer from the catalyst to the oxidant, transfer of a hydroxy radical from the oxidant to the catalyst can take place. This results a shunt pathway in the actual water oxidation mechanism. Consequently several researchers decided to use other oxidants for chemical catalytic water oxidation. Periodate is an interesting alternative to CAN as it is a much weaker oxidant and is stable under mild conditions[6b,14] (the redox potential of CAN is 1.8 V at pH 0, while the redox potential of periodate at pH 7 is 1.2 V).[14d] However, periodate does contain atomic oxygen and in theory could produce O_2 in the absence of water. If this is the case, periodate is obviously not a good model for the study of catalytic water oxidation, even though some of the catalytic intermediates may be the same. It is difficult

[a] Currently at Leiden Institute of Chemistry, Leiden University, P. O. Box 9502, 2300 RA Leiden, The Netherlands
E-mail: d.g.h.hetterscheid@chem.leidenuniv.nl
http://casc.lic.leidenuniv.nl/
[b] Van 't Hoff Institute for Molecular Sciences, University of Amsterdam,
P. O. Box 94720, 1090 GE Amsterdam, The Netherlands
Supporting information for this article is available on the WWW under http://dx.doi.org/10.1002/ejic.201300249.

to verify experimentally whether O_2 production is actually the result of catalytic water oxidation or decomposition of periodate. Both reactions have the same overall stoichiometry, and because of the equilibrium of IO_4^- with water to produce $H_4IO_6^-$, ^{18}O-labeling experiments to identify whether dioxygen production originates from water oxidation or periodate decomposition are inconclusive (Figure 1).[14a,15] Although periodate was expected to act as a one-electron oxidant in catalytic water oxidation reactions, experimental evidence of such a one-electron pathway has been reported only once.[16] Examples of inner-sphere two-electron oxidations and O-atom transfer[17] are much more common. Even though the pathway of oxidation is ambiguous, the use of periodate as a chemical oxidant in catalytic water oxidation is becoming increasingly popular. In the case of several IrCp* complexes[14a] beside [IrCp*(Me$_2$NHC)(OH)$_2$] {**Ir**(OH)$_2$} (see below), dioxygen production was observed upon addition of periodate in water {**Ir** = [IrCp*(Me$_2$NHC)], where Me$_2$NHC = *N*-dimethylimidazolin-2-ylidene and Cp* = cyclopentadienyl}. Intrigued by the noninnocence of periodate, and prompted by the idea that O_2 production might proceed via two O-atom-transfer reactions instead of catalytic oxidation of water, we investigated such a pathway by in situ mass spectroscopy experiments and with DFT for **Ir**(OH)$_2$. In this paper we demonstrate that when periodate is used as the chemical oxidant: (1) a water-independent pathway for O_2 evolution exists in the presence of **Ir**, and (2) that "O"-atom-transfer shunts are readily accessible. We expect that these findings will prove relevant to several more water oxidation catalysts when periodate is used as the chemical oxidant.

water oxidation:

$$2\,IO_4^- + 2\,H_2O \longrightarrow 2\,IO_3^- + O_2 + 2\,H_2O$$

periodate decomposition:

$$2\,IO_4^- \longrightarrow 2\,IO_3^- + O_2$$

periodate equilibrium resulting in scrambling of the ^{18}O label:

$$2\,IO_4^- + 2\,H_2O \rightleftharpoons 2\,H_4IO_6^-$$

Figure 1. Oxygen labeling and the mechanism of catalytic water oxidation: (top) both oxygen atoms in the formed dioxygen molecule originate from water; (middle) periodate decomposition, wherein one or both oxygen atoms in the dioxygen stem from periodate instead, and (bottom) the equilibrium between *ortho*- and *meta*-periodate results in fast scrambling of oxygen.[15]

Results and Discussion

In a previous communication we mentioned that **Ir**(OH)$_2$ is a catalyst for water oxidation, both electrochemically and in the presence of CAN as a stoichiometric oxidant. Catalytic intermediates pointing to a molecular active species have been observed by ESI-MS.[4f] In the present case, dioxygen evolution on treatment of **Ir**(OH)$_2$ with $NaIO_4$ in water, and with [NBu$_4$]IO_4 in organic solvents, was studied. In the absence of water, no O_2 formation was observed. Addition of small amounts of water to a 100 mM periodate solution in dichloromethane in the presence of 1 mM catalyst resulted in formation of a purple solution and formation of small amounts of O_2. These events occurred predominantly in small water pockets that separated from the dichloromethane solution. In polar organic solvents such as acetonitrile and DMF large amounts of water were required before any O_2 evolution, which never occurred in large quantities. When **Ir**(OH)$_2$ was treated in water, immediate evolution of O_2 was observed. The reaction of **Ir**(OH)$_2$ with periodate was studied with a Clark electrode in the liquid phase; very diluted iridium concentrations were used and initial rates recorded, minimizing possible involvement of iridium oxo nanoparticles,[18] which are formed relatively slowly for IrCp* complexes, even the [IrCp*(OH$_2$)$_3$]$^{2+}$ parent complex.[14c] A turnover frequency of 0.27 s^{-1} was observed at 27 μM **Ir**(OH)$_2$ and 274 mM $NaIO_4$ concentrations, and a broken rate order of 0.51 in $NaIO_4$ and 0.65 in catalyst was found (Figure 2). When CAN was used as a chemical oxidant a turnover frequency of 0.43 s^{-1} and a first-order dependence on both CAN and

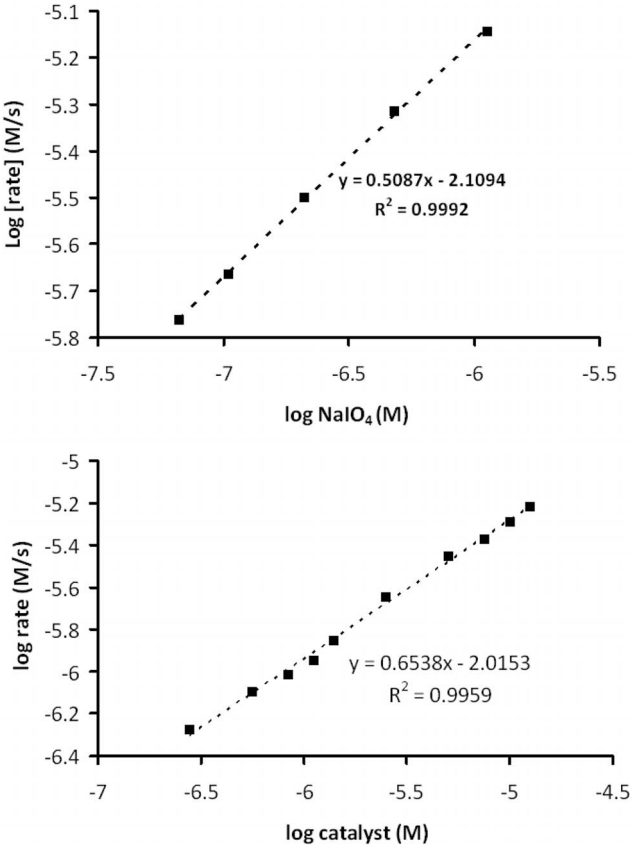

Figure 2. Log–log plots of the rate as a function of the periodate and the catalyst concentration. (Top) The $NaIO_4$ concentration was varied between 16 mM and 270 mM while the **Ir**(OH)$_2$ concentration was fixed at 27 μM. (Bottom) The **Ir**(OH)$_2$ concentration was varied between 0.5 μM and 25 μM while the $NaIO_4$ concentration was fixed at 234 mM. From these plots a rate law of $v = k_{obs}[\mathbf{Ir}]^{0.65}[IO_4]^{0.5}$ was deduced, with $k_{obs} = 1.5 \times 10^{-3}$ and a turnover frequency of 0.27 s^{-1} at 237 mM $NaIO_4$ and 27 μM **Ir**(OH)$_2$ concentration.

catalyst were observed. **Ir**$(OH)_2$ partly dimerizes at high pH, and this dimerization may have caused the fractional order dependence on catalyst at pH 7. The order of 0.5 with respect to periodate points to a one-electron oxidation as the rate-determining step, like the first-order dependence on CAN. Addition of iodate did not inhibit the catalytic reaction.

In order to unravel the mechanism of O_2 production at **Ir**$(OH)_2$, in situ mass spectrometry measurements were carried out. Treatment of **Ir**$(OH)_2$ with iodate results in formation of iodate complexes. Whereas relatively large signals at *m*/*z* = 441 and 481, corresponding to [**Ir**$(OH)]^+$ and [**Ir**$(OH)_2$ + Na$]^+$, were observed in the absence of iodate,[4f] addition of iodate to **Ir**$(OH)_2$ resulted in formation of new species (Figure 3, top). The signals at *m*/*z* = 689, 707, and 725 confirm the formation of the iodate complex [**Ir**$(IO)_3]^+$ with 5, 6, and 7 additional water molecules present. In addition, a signal is seen at *m*/*z* = 847, which corresponds to a protonated bisiodate complex and four water molecules. Apparently, iodate is a good ligand for **Ir**. When **Ir**$(OH)_2$ is treated with sodium periodate, a more complicated mixture of products is observed (Figure 3, bottom). The signal at *m*/*z* = 389 indicates formation of the same [**Ir**$(IO_3)]^+$ complex, suggesting that this species may be important in the catalytic mechanism of O_2 production. The signals at *m*/*z* = 705 and 723 correspond to the "periodate" [**Ir** + I + 4O$]^+$ species with five and six water molecules. If periodate indeed coordinates to iridium, it seems likely that oxidation proceeds via O-atom transfer. However, it is important to note that these signals may also correspond to iodate complexes that have been oxidized at the metal site. Finally, the signals at *m*/*z* = 703 and 721 point to species that have been even further oxidized.

Since the ESI-MS data point to coordination of iodate and periodate, these species were investigated by means of DFT calculations. Remarkably, optimization of [**Ir**$(IO_4)]^+$ did not result in a stable species, and spontaneous I–O bond cleavage occurred, resulting in [**Ir**$(=O)(IO_3)]^+$. For this species it was found that the triplet state was slightly lower in energy than the singlet state, while a broken symmetry optimization did not afford new species. Only when a constraint was placed on the I–O bond did the calculation converge to [**Ir**$(IO_4)]^+$. The I–O bond scission was calculated to be exergonic by 25.4 kcal/mol. Hence, the species that was observed by ESI-MS cannot have been [**Ir**$(IO_4)]^+$; [**Ir**$(=O)(IO_3)]^+$ seems to be a much better candidate. Since [**Ir**$(IO_3)]^+$ and most likely [**Ir**$(=O)(IO_3)]^+$ have been observed, a catalytic pathway involving both these species was

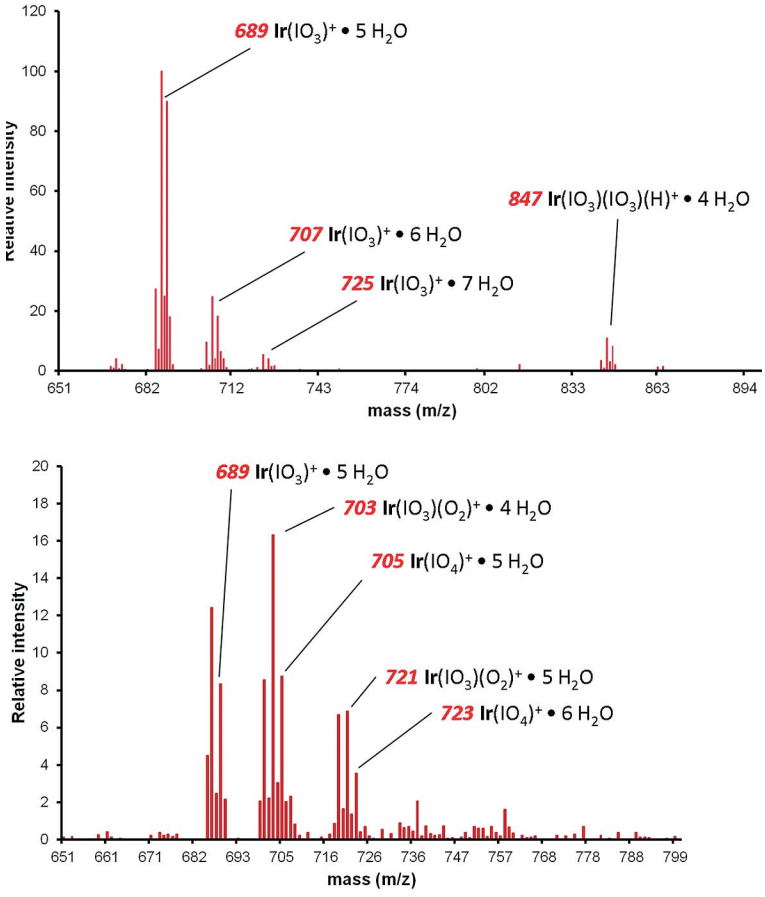

Figure 3. (Top) ESI-MS spectra of **Ir**$(OH)_2$ after treatment with $NaIO_3$. The observed signals are consistent with formation of [**Ir**$(IO_3)]^+$ and **Ir**$(IO_3)_2$ species. No signs of **Ir**$(OH)_2$ have been observed in the ESI-MS. (Bottom) Treatment of **Ir**$(OH)_2$ with $NaIO_4$ results in formation of a mixture of species. Beside masses that correspond to [**Ir** + I + 4O$]^+$, species that have lost or gained an oxygen atom are also present.

investigated by DFT calculations. Although the first turnover cannot include iodate, $[\mathbf{Ir}(IO_3)]^+$ was chosen as the starting point of the catalytic pathway and its energy was used as a reference point (Figure 4). It was found that the $[\mathbf{Ir}(IO_4)]^+$ species with an O–I constraint of 2.0 Å was 24.1 kcal/mol higher in energy and thus inaccessible from $[\mathbf{Ir}(IO_3)]^+$. Formation of $[\mathbf{Ir}(IO_4)]^+$ therefore could only occur, if at all, at the initiation or very early stage of the catalytic reaction when the IO_3^- concentration is very low. Cleavage of one of the Ir–O bonds of the chelate $[\mathbf{Ir}(IO_3)]^+$ results in formation of a vacant site at iridium. This reaction is uphill by only 1.1 kcal/mol and thus can take place readily. Coordination of periodate to this species yields neutral $\mathbf{Ir}(IO_3)(IO_4)$, requiring 14.2 kcal/mol. Comparison of neutral complexes with charged complexes in these gas-phase calculations is difficult and gives rise to a relatively large error, despite the COSMO solvent corrections that were applied. For neutral $\mathbf{Ir}(IO_3)(IO_3)$ a relatively high energy of 8.0 kcal/mol was found, although this species was observed experimentally by ESI-MS. Probably the entropy change of coordination of iodate in these relatively concentrated iodate solutions is overestimated by these gas-phase calculations. Hence, the calculated energy of $\mathbf{Ir}(IO_3)(IO_4)$ is probably too high as well. O-atom transfer from periodate to the iridium complex via cleavage of the I–O bond results in facile formation of $[\mathbf{Ir}(=O)(IO_3)]^+$ and IO_3^- via a very broad and low barrier that consequently was impossible to find. From stepwise elongation of the I–O bond it was estimated that the barrier must be 2–3 kcal/mol at most. O–O bond formation by coupling of the oxo fragment of $[\mathbf{Ir}(=O)(IO_3)]^+$ with periodate was found to proceed over a very high barrier with an enthalpy of 35 kcal/mol. Since such a huge enthalpy change was found, no hessian was calculated for this transition state. Given the bimolecular nature of this reaction, the entropy contribution is expected to further increase the total Gibbs free energy. To circumvent this, an intramolecular nucleophilic attack of periodate was considered. Displacement of iodate at $[\mathbf{Ir}(=O)(IO_3)]^+$ by periodate to form $[\mathbf{Ir}(=O)(IO_4)]^+$ was found to be uphill by 9 kcal/mol. The transition state of the subsequent intramolecular O–O bond formation was found at 45 kcal/mol (singlet TS) or 38 kcal/mol (triplet TS) and is not accessible at room temperature. Remarkably, the singlet transition state of intramolecular nucleophilic attack of iodate on the oxo fragment was found at a much lower energy at 20.5 kcal/mol. This O–O bond formation results in formation of a IrOOIO pentacycle, which was found at 15.6 kcal/mol. The unexpected large difference in transition-state energy between O–O bond formation at $[\mathbf{Ir}(=O)(IO_4)]^+$ and $[\mathbf{Ir}(=O)(IO_3)]^+$ is most likely the result of iodate being a much better nucleophile than periodate. The intramolecular nucleophilic attack on the Ir(=O) moiety, which has an electrophilic character, is much easier for the iodate complex. Whereas $\{\mathbf{Ir}[OOI(O)O]\}^+$ has a local minimum as a singlet species, triplet $\{\mathbf{Ir}[OOI(O)O]\}^+$ immediately opens an I–O bond, forming transient $[\mathbf{Ir}(IO_2)(\eta^1\text{-}O_2)]^+$. For this reaction,

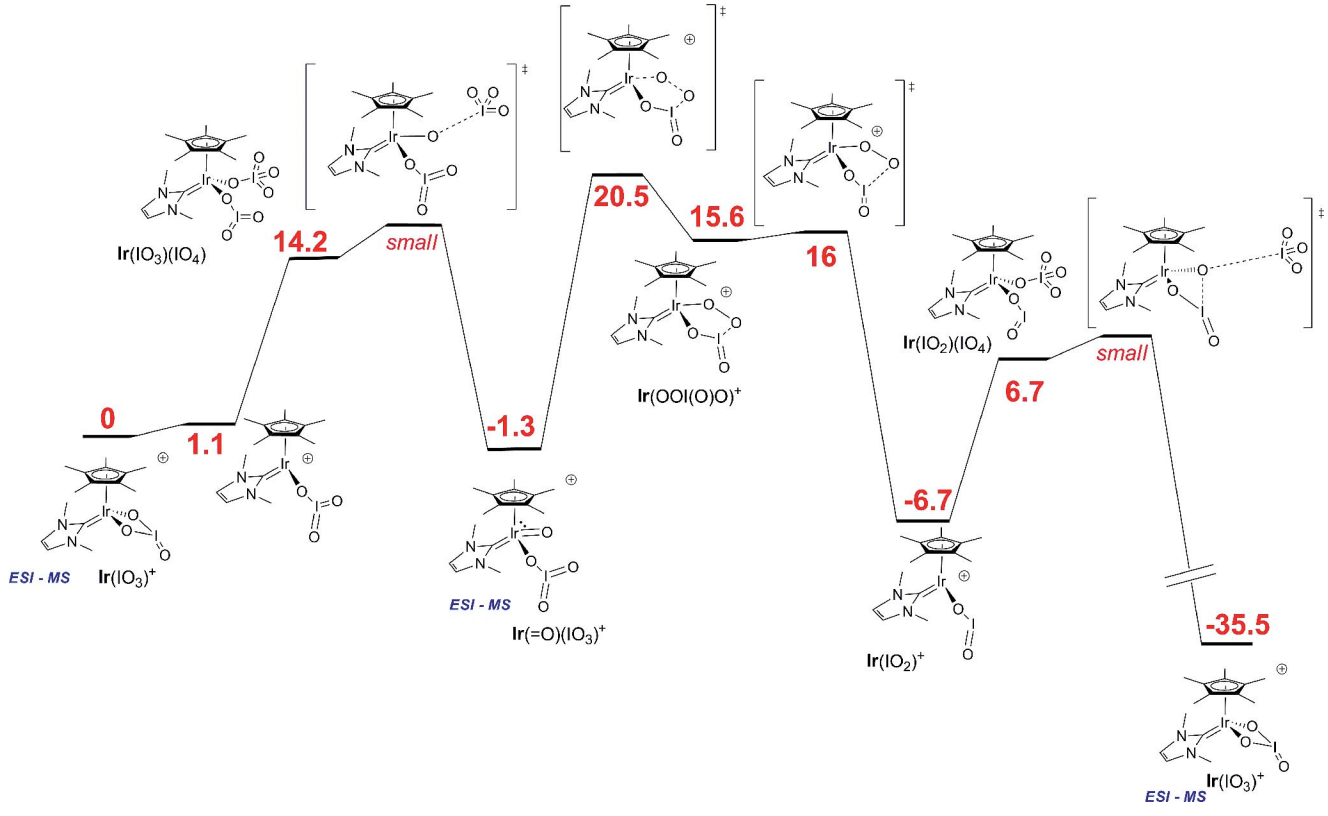

Figure 4. Calculated pathway of water-independent O_2 generation from periodate mediated by $[\mathbf{Ir}(IO_3)]^+$ species. Energies are in kcal/mol.

a spin crossover point was found at 16 kcal/mol. This transition state is an upper limit for the crossover of the singlet to the triplet state and the $\{\mathbf{Ir}[OOI(O)O]\}^+$ species therefore must be very labile. The Mullikin spin distribution analysis of the resulting $[\mathbf{Ir}(IO_2)(\eta^1\text{-}O_2)]^+$ species revealed that most spin density of the unpaired electrons is located on both O atoms of the O_2 ligand. [Complex $\mathbf{Ir}(IO_2)(\eta^1\text{-}O_2)]^+$ is therefore best described as an iridium(III) species with a side-on coordinated dioxygen ligand rather than an iridium(IV) superoxide complex. This $[\mathbf{Ir}(IO_2)(\eta^1\text{-}O_2)]^+$ species spontaneously decoordinates dioxygen in a barrierless reaction producing $[\mathbf{Ir}(IO_2)]^+$ and triplet dioxygen. The $[\mathbf{Ir}(IO_2)]^+$ species was found at –6.7 kcal/mol relative to $[\mathbf{Ir}(IO_3)]^+$. Dissociation of free iodite is thermodynamically not feasible, and $[\mathbf{Ir}(IO_2)]^+$ must therefore be relatively stable in the absence of any periodate. In the presence of excess periodate, coordinated iodite is believed to undergo a very facile comproportionation reaction to produce iodate. Coordination of periodate to $[\mathbf{Ir}(IO_2)]^+$ results in $\mathbf{Ir}(IO_2)(IO_4)$ in an uphill reaction of 13.4 kcal/mol. As for $\mathbf{Ir}(IO_3)_2$ and $\mathbf{Ir}(IO_3)(IO_4)$, this energy change is probably overestimated.

Cleavage of the I–O bond of coordinated periodate of $\mathbf{Ir}(IO_4)(IO_2)$ proceeds over a very low and broad barrier (1–4 kcal/mol) resulting in formation of $\mathbf{Ir}(IO_3)$ via a concerted O–I bond formation with exclusion of IO_3^- and closes the catalytic cycle. The overall energy of O_2 formation from periodate corresponds very well to the experimentally values (DFT: –35.5, experimental: –33.2 kcal/mol).[19] It is important to note that metaperiodate complexes did not converge, and coordination of water to **Ir** simultaneously with iodate resulted in spontaneous decoordination of water during optimization.

As an alternative to intramolecular nucleophilic attack of iodate on the metal oxo fragment of $[\mathbf{Ir}(=O)(IO_3)]^+$, nucleophilic attack of water from the solution was considered too (Figure 5). For the O–O bond formation we found a transition state of 35 kcal/mol, which is too high in energy to explain the observed O_2 production rates. However, the entropy contribution of the bimolecular reaction of water is probably greatly exaggerated in these gas-phase calculations, since water is abundantly present as it is the solvent. The enthalpy of 28 kcal/mol for the transition state is probably a more meaningful number. As the water carries out its nucleophilic attack on the metal oxo moiety, it also forms a hydrogen bond with the iodate ligand. During formation of the O–O bond, the proton is transferred from water to the iodate ligand, preventing formation of an $Ir\text{–}O\text{–}OH_2$ species. Similarly, in the case of other iridium and ruthenium water oxidation catalysts, DFT calculations suggest that formation of a metal–$O\text{–}OH_2$ species must be avoided to obtain a low-lying transition state.[20] In our approximation the iridium center eventually coordinates a HIO_3 ligand. The proton of coordinated periodic acid must be very acidic and at pH 7 is probably lost to the solution simultaneously with O–O bond formation. Addition of base as a buffer to a periodate/**Ir** solution to promote this O–O bond formation step resulted in significantly higher rates.[21] However, this trend was also visible in the control experiments and may be an effect of the base on the stability or redox potential of periodate instead. In line with the apparent importance of stabilizing the proton, incorporation of additional water molecules in the transition state have significantly reduced the transition state energy in the case of IrCp*(phenylpyrine) catalysts.[4b] In the case of nucleophilic attack by water on $[\mathbf{Ir}(=O)(IO_3)]^+$, addition of one or two extra water molecules did not reduce the energy of this transition state.

The apparent requirement of water for the formation of dioxygen seems to point to an important role for water in the catalytic mechanism. However, the lack of O_2 formation in organic solvents may also be the result of inhibition of the catalytic site by the organic solvent (e.g. MeCN, DMF) or low stability of charged intermediates in solution, and consequently slow ligand-exchange kinetics. The observation of $[\mathbf{Ir} + I + 3O]^+$ and $[\mathbf{Ir} + I + 4O]^+$ species in the ESI-MS spectra fits very nicely with the mechanism outlined in Figure 4, where $[\mathbf{Ir}(IO_3)]^+$ and $[\mathbf{Ir}(=O)(IO_3)]^+$ are the low-energy states. It therefore seems likely that these species are involved in catalytic O_2 production mediated by **Ir**. Also, the DFT calculations illustrate that iodate is not an inhibitor, as coordination of iodate to $[\mathbf{Ir}(IO_3)]^+$ seems to be an uphill reaction, which is in agreement with kinetic experiments in the presence of excess iodate. Nevertheless, the observed reaction kinetics do not entirely match the mechanism outlined in Figure 4. In this scheme the rate-determining step is periodate-independent O–O bond formation at $[\mathbf{Ir}(=O)(IO_3)]^+$, which is preceded by a periodate-dependent equilibrium. Since the concentration of periodate is very large relative to that of the catalyst, we would have expected a zero-order dependence or saturation kinetics for periodate. Instead a rate dependence with respect to periodate was found that fits best to a half-order dependence. Also, the twofold O-atom-transfer pathway described in Figure 4 does not explain formation of the $[\mathbf{Ir} + I + 5O]^+$ species. This species could be the result of ligand-based oxidation reactions,[22] but may also be a species such as $[\mathbf{Ir}(\eta^1\text{-}O_2)(IO_3)]^+$. According to DFT calculations, $[\mathbf{Ir}(\eta^1\text{-}O_2)(IO_3)]^+$ behaves similarly to $[\mathbf{Ir}(\eta^1\text{-}O_2)(IO_2)]^+$, and is best described as an iridium(III) species with a coordinated dioxygen ligand on the basis of Mullikin spin-population analysis. In the absence of constraints, the complex spontaneously loses the dioxygen ligand. It is therefore impossible that this species would be present in solution in sufficiently large amounts be trapped with ESI-MS. The alternative structure in which the O_2 fragment is coordinated side-on to the iridium center seems to be a better candidate, as this iridium(V) peroxide species is thermodynamically stable. However, it is not clear how this species is formed instead of the transient iridium(III)–dioxygen species as a result of the water nucleophilic attack mechanism outlined in Figure 5.

The observed transition state of 21.8 kcal/mol found for O_2 evolution via two subsequent O-atom-transfer reactions fits well with the observed turnover frequency of 0.27 s^{-1}. This illustrates that, even though this may not necessarily be the dominant pathway under the conditions studied, it may very well be a relevant route. The first O-atom transfer

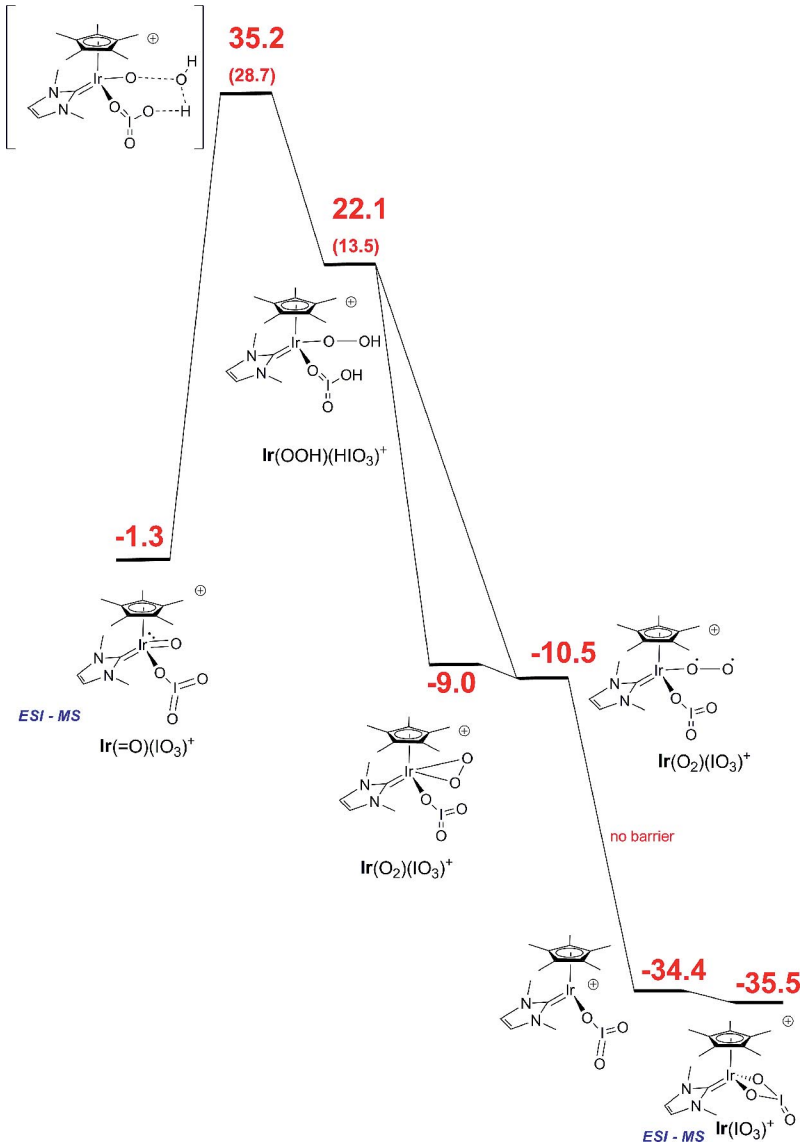

Figure 5. Water nucleophilic attack mechanism at [**Ir**(=O)(IO_3)]$^+$. Energies are in kcal/mol; enthalpies are given in parentheses.

in particular is facile, and this part of the catalytic cycle may in fact be the dominant route. It is important to note that the barrier of 21.8 kcal/mol is very similar to the barriers of other water oxidation mechanisms that proceed exclusively by one-electron-transfer oxidation steps; these barriers have been calculated for related iridium and ruthenium water oxidation catalysts as 16–24 kcal/mol.[20] Comparing these numbers, one may expect that catalytic periodate decomposition is in competition with catalytic water oxidation in several cases beside that of **Ir**. DFT calculations of the full catalytic water oxidation cycle of **Ir**($OH)_2$ in the absence of (coordinated) iodate and periodate are currently in progress and will be reported in due course.

Conclusions

We have studied periodate-driven iridium-catalyzed water oxidation with a combined experimental and theoretical approach. Although the dominant mechanism of O_2 evolution has not been unambiguously established, the DFT calculations show that a low-lying pathway exists in which O_2 production occurs without direct involvement of water. In particular, coordination of periodate to the relatively electron-rich intermediates of the catalytic cycle and O-atom transfer from coordinated periodate to iridium were found to be very facile. In the calculated mechanism, the key O–O bond formation takes place at a metal oxo species, which undergoes nucleophilic attack by iodate. Like periodate, iodate is clearly not an innocent species in these periodate-driven water oxidation reactions. Although the intramolecular O–O bond formation step is limited to catalytic species that have two labile sites, it is very likely that these types of reactions are *not* limited to the iridium catalyst studied in the present work, and it is expected that similar events occur for many other water oxidation catalysts in the presence of periodate. This holds especially for the

O-atom-transfer steps. Therefore, one has to be very careful when interpreting results while studying catalytic water oxidation with periodate as a chemical oxidant.

Experimental Section

General: The complex **Ir**$(OH)_2$[4f] and $[Bu_4N]IO_4$[23] were prepared by literature procedures. ESI mass spectra were recorded with a Shimadzu LCMS-2010A; the samples were directly injected into the mass spectrometer.

Catalytic Experiments: Water oxidation experiments were carried out in a Hansatech Oxygraph reactor equipped with a Clark electrode. The reactor was left open to the atmosphere as it was used only for determination of initial rates of catalytic activity. Within a series of experiments the Clark electrode proved very accurate, as perfect reproducibility was observed. However, between different sets of experiments, after which the Clark electrode was prepared and recalibrated, rates compared to previous experiments were initially off. Eventually this problem was solved by rigorously cleaning the electrode after every series of measurements. Nevertheless all measurements carried out were calibrated to **Ir**$(OH)_2$ under standard conditions (10 μM catalyst; 100 mM CAN) to ensure reproducibility. All experiments were carried out three times, except for **Ir**$(OH)_2$ under standard conditions, which was measured more often and was also repeated throughout a series of other measurements to rule out drifting of the device. In a typical experiment, CAN or $NaIO_4$ solution (1 mL) was placed in the vessel equipped with the Clark electrode and stock solution of catalyst (≈ 1–10 μM, 1 mL) was added. To ensure that the solution was homogeneous the liquid was stirred vigorously by injection and ejection of the material by syringe. Typically, O_2 production started immediately after the short mixing time (10 s).

DFT Calculations: All geometry optimizations were carried out with the Turbomole program[24] coupled to the PQS Baker optimizer.[25] Geometries were fully optimized as minima at the bp86 level[26] using the Turbomole SV(P) basis set[27] on all atoms. The obtained structures were further optimized at the b3-lyp level[28] using the TZVP basis.[26,27c,29] The solvent effects of water were computed with the COSMO model[30] by further optimization of the gas-phase optimized geometries, using the same basis set. Frequency calculations were used to determine the zero-point, thermal, and entropy contributions to the energy.

Supporting Information (see footnote on the first page of this article): Kinetic data and the calculated coordinates of the DFT geometry optimizations.

Acknowledgments

The authors thank Dr. Bas De Bruin for tricks and tips concerning the DFT calculations. This work was supported by the Netherlands Organization for Scientific Research (NWO-CW, VENI grant 700.59.410).

[1] Intergovernmental Panel on Climate Change, *IPCC Fourth Assessment Report*, **2007**, Working Group III, chapter 4.

[2] a) N. S. Lewis, D. G. Nocera, *Proc. Natl. Acad. Sci. USA* **2006**, *103*, 15279; b) D. G. H. Hetterscheid, J. I. Van der Vlugt, B. De Bruin, J. N. H. Reek, *Angew. Chem.* **2009**, *121*, 8324; *Angew. Chem. Int. Ed.* **2009**, *48*, 8178; c) N. D. McDaniel, S. Bernhard, *Dalton Trans.* **2010**, *39*, 10021.

[3] a) J. J. Concepcion, J. W. Jurss, J. L. Templeton, T. J. Meyer, *J. Am. Chem. Soc.* **2008**, *130*, 16462; b) D. J. Wasylenko, C. Ganesamoorthy, M. A. Henderson, B. D. Koivisto, H. D. Osthoff, C. P. Berlinguette, *J. Am. Chem. Soc.* **2010**, *132*, 16094; c) J. J. Concepcion, M.-K. Tsai, J. T. Muckerman, T. J. Meyer, *J. Am. Chem. Soc.* **2010**, *132*, 1545; d) M. Yagi, S. Tajima, M. Komi, H. Yamazaki, *Dalton Trans.* **2011**, *40*, 3802; e) N. Kaveevivitchai, R. Zong, H.-W. Tseng, R. Chitta, R. P. Thummel, *Inorg. Chem.* **2012**, *41*, 2930; f) D. E. Polyansky, J. T. Muckerman, J. Rochford, R. Zong, R. P. Thummel, E. Fujita, *J. Am. Chem. Soc.* **2011**, *133*, 14649; g) X. Sala, M. Z. Ertem, L. Vigara, T. K. Todorova, W. Chen, R. C. Rocha, F. Aquilante, C. J. Cramer, L. Gagliardi, A. Llobet, *Angew. Chem.* **2010**, *122*, 7911; *Angew. Chem. Int. Ed.* **2010**, *49*, 7745; h) L. Duan, A. Fischer, Y. Xu, L. Sun, *J. Am. Chem. Soc.* **2009**, *131*, 10397; i) L. Tong, L. Duan, Y. Xu, T. Privalov, L. Sun, *Angew. Chem.* **2011**, *123*, 465; *Angew. Chem. Int. Ed.* **2011**, *50*, 445.

[4] a) N. D. McDaniel, F. J. Coughlin, L. L. Tinker, S. Bernhard, *J. Am. Chem. Soc.* **2008**, *130*, 210; b) J. D. Blakemore, N. D. Schley, D. Balcells, J. F. Hull, G. W. Olack, C. Incarvito, O. Eisenstein, G. W. Brudvig, R. H. Crabtree, *J. Am. Chem. Soc.* **2010**, *132*, 16017; c) J. F. Hull, D. Balcells, J. D. Blakemore, C. D. Incarvito, O. Eisenstein, G. W. Brudvig, R. H. Crabtree, *J. Am. Chem. Soc.* **2009**, *131*, 8730; d) T. P. Brewster, J. D. Blakemore, N. D. Schley, C. D. Incarvito, N. Hazari, G. W. Brudvig, R. H. Crabtree, *Organometallics* **2011**, *30*, 965; e) R. Lalrempuia, N. D. McDaniel, H. Muller-Bunz, S. Bernhard, M. Albrecht, *Angew. Chem.* **2010**, *122*, 9959; *Angew. Chem. Int. Ed.* **2010**, *49*, 9765; f) D. G. H. Hetterscheid, J. N. H. Reek, *Chem. Commun.* **2011**, *47*, 2712; g) A. Savini, G. Bellachioma, G. Ciancaleoni, C. Zuccaccia, D. Zuccaccia, A. Macchioni, *Chem. Commun.* **2010**, *46*, 9218; h) A. Savini, G. Bellachioma, S. Bolano, L. Rocchigiani, C. Zuccaccia, D. Zuccaccia, A. Macchioni, *ChemSusChem* **2012**, *5*, 1415; i) A. Bucci, A. Savini, L. Rocchigiani, C. Zuccaccia, S. Rizzato, A. Albinati, A. Llobet, A. Macchioni, *Organometallics* **2012**, *31*, 8071.

[5] a) J. Limburg, J. S. Vrettos, H. Chen, J. C. de Paula, R. H. Crabtree, G. W. Brudvig, *J. Am. Chem. Soc.* **2001**, *123*, 423–430; b) Y. Gao, R. H. Crabtree, G. W. Brudvig, *Inorg. Chem.* **2012**, *51*, 4043; c) R. Brimblecombe, G. F. Swiegers, G. C. Dismukes, S. Spiccia, *Angew. Chem.* **2008**, *120*, 7445; *Angew. Chem. Int. Ed.* **2008**, *47*, 7335.

[6] a) W. C. Ellis, N. D. McDaniel, S. Bernhard, T. J. Collins, *J. Am. Chem. Soc.* **2010**, *132*, 10990; b) J. L. Fillol, Z. Codola, I. Garcia-Bosch, L. Gomez, J. J. Pla, M. Costas, *Nature Chem.* **2011**, *3*, 807.

[7] a) D. J. Wasylenko, C. Ganesamoorthy, J. Borau-Garcia, C. P. Berlinguette, *Chem. Commun.* **2011**, *47*, 4249; b) D. Kogutan, R. McGuire, D. G. Nocera, *J. Am. Chem. Soc.* **2011**, *133*, 9178.

[8] a) S. M. Barnett, K. I. Goldberg, J. M. Mayer, *Nat. Chem.* **2012**, *4*, 498; b) Z. Chen, T. J. Meyer, *Angew. Chem.* **2013**, *125*, 728; *Angew. Chem. Int. Ed.* **2013**, *52*, 700.

[9] J. J. Concepcion, J. W. Jurss, P. G. Hoertz, T. J. Meyer, *Angew. Chem.* **2009**, *121*, 9637; *Angew. Chem. Int. Ed.* **2009**, *48*, 9473.

[10] L. Duan, F. Bozoglian, S. Mandal, B. Stewart, T. Privalov, A. Llobet, L. Sun, *Nat. Chem.* **2012**, *4*, 418.

[11] a) D. G. H. Hetterscheid, J. N. H. Reek, *Angew. Chem.* **2012**, *124*, 9878; *Angew. Chem. Int. Ed.* **2012**, *51*, 9740; b) D. J. Wasylenko, R. D. Palmer, C. P. Berlinguette, *Chem. Commun.* **2013**, *49*, 218; c) R. Cao, W. Lai, P. Du, *Energy Environ. Sci.* **2012**, *5*, 8134.

[12] a) D. J. Wasylenko, C. Ganesamoorthy, M. A. Henderson, C. P. Berlinguette, *Inorg. Chem.* **2011**, *50*, 3662; b) N. G. Connelly, W. E. Geiger, *Chem. Rev.* **1996**, *96*, 877.

[13] M. Yoshida, S. Masaoka, J. Abe, K. Sakai, *Chem. Asian J.* **2010**, *5*, 2369.

[14] a) A. R. Parent, T. P. Brewster, W. De Wolf, R. H. Crabtree, G. W. Brudvig, *Inorg. Chem.* **2012**, *51*, 6147; b) A. R. Parent, J. D. Blakemore, G. W. Brudvig, R. H. Crabtree, *Chem. Commun.* **2011**, *47*, 11745; c) U. Hintermair, S. M. Hashmi, M. Eli-

melech, R. H. Crabtree, *J. Am. Chem. Soc.* **2012**, *134*, 9785; d) A. R. Parent, R. H. Crabtree, G. W. Brudvig, *Chem. Soc. Rev.* **2013**, *42*, 2247.
[15] Exchange of IO_4^- with $H_2{}^{17}O$ proceeds via a pseudo-first-order rate law with respect to IO_4^-, with $k_{obs} = 1200\ s^{-1}$; i.e. the half-life of periodate scrambling is in the order of milliseconds! See: I. Pecht, Z. Luz, *J. Am. Chem. Soc.* **1965**, *87*, 4068.
[16] F. R. El-Eziri, Y. Sulfab, *Inorg. Chim. Acta* **1977**, *25*, 15.
[17] a) J. Mei, K. M. Carsch, C. R. Freitag, T. B. Gunnoe, T. R. Cundari, *J. Am. Chem. Soc.* **2013**, *135*, 424; b) K. N. Naik, S. T. Nandibewoor, *Catal. Sci. Technol.* **2011**, *1*, 1232; c) M. A. Hussain, A. A. Abdel-Khalek, Y. Sulfab, *J. Chem. Soc., Dalton Trans.* **1983**, 317; d) P. Pietikainen, *Tetrahedron Lett.* **1995**, *36*, 319; e) S. Roth, S. Göhler, H. Cheng, C. B. W. Stark, *Eur. J. Org. Chem.* **2005**, 4109.
[18] a) D. B. Grotjahn, D. B. Brown, J. K. Martin, D. C. Marelius, M.-C. Abadjian, H. N. Tran, G. Kalyuzhny, K. S. Vecchio, Z. G. Specht, S. A. Cortes-Llamas, V. Miranda-Soto, C. Van Niekerk, C. E. Moore, A. L. Rheingold, *J. Am. Chem. Soc.* **2011**, *133*, 19024; b) D. Hong, M. Murakami, Y. Yamada, S. Fukuzumi, *Energy Environ. Sci.* **2012**, *5*, 5708; c) R. H. Crabtree, *Chem. Rev.* **2012**, *112*, 1536.
[19] a) D. D. Wagman, W. H. Evans, V. B. Parker, R. H. Schumm, I. Halow, S. M. Bailey, K. L. Churney, R. L. Nuttall, *NBS Tables of Chemical Thermodynamic Properties, J. Phys. Chem. Ref. Data*, **1982**, vol. 11, Suppl. 2; b) J. F. Zemaitis, D. M. Clark, M. Rafal, N. C. Scrivner, *Handbook of Aqueous Electrolyte Thermodynamics*, American Institute of Chemical Engineers, New York, **1986**.
[20] a) T. F. Hughes, R. A. Friesner, *J. Phys. Chem. B* **2011**, *115*, 9280; b) L. Vilella, P. Vidossich, D. Balcells, A. Lledos, *Dalton Trans.* **2011**, *40*, 11241; c) J. L. Valles-Pardo, M. C. Guijt, M. Iannuzzi, K. S. Joya, H. J. M. De Groot, F. Buda, *ChemPhysChem* **2012**, *13*, 140.
[21] Z. Chen, J. J. Concepcion, X. Hu, W. Yang, P. G. Hoertz, T. J. Meyer, *Proc. Natl. Acad. Sci. USA* **2010**, *107*, 7225.
[22] a) C. Zuccaccia, G. Bellachioma, S. Bolano, L. Rocchigiani, A. Savini, A. Macchioni, *Eur. J. Inorg. Chem.* **2012**, 1462; b) A. Savini, P. Belanzoni, G. Bellachioma, C. Zuccaccia, D. Zuccaccia, A. Macchioni, *Green Chem.* **2011**, *13*, 3360.
[23] K. Inomata, Y. Nakayama, H. Kotake, *Bull. Chem. Soc. Jpn.* **1980**, *53*, 565.
[24] R. Ahlrichs, M. Bär, H.-P. Baron, R. Bauernschmitt, S. Bocker, M. Ehrig, K. Eichkorn, S. Elliott, F. Furche, F. Haase, M. Haser, C. Hattig, H. Horn, C. Huber, U. Huniar, M. Kattannek, A. Kohn, C. Kolmel, M. Kollwitz, K. May, C. Ochsenfeld, H. Ohm, A. Schafer, U. Schneider, O. Treutler, K. Tsereteli, B. Unterreiner, M. Von Arnim, F. Weigend, P. Weis, H. Weiss, *Turbomole*, v. 5, Theoretical Chemistry Group, University of Karlsruhe, Germany, **2002**.
[25] J. Baker, *J. Comput. Chem.* **1986**, *7*, 385.
[26] a) A. D. Becke, *Phys. Rev. A* **1988**, *38*, 3089; b) J. P. Perdew, *Phys. Rev. B* **1986**, *33*, 8822.
[27] a) Turbomole basis set library, Turbomole Version 5, see ref.[23]; b) A. Schafer, H. Horn, R. Ahlrichs, *J. Chem. Phys.* **1992**, *97*, 2571; c) D. Andrae, U. Häussermann, M. Dolg, H. Stoll, H. Preuss, *Theor. Chim. Acta* **1990**, *77*, 123.
[28] a) C. Lee, W. Yang, R. G. Parr, *Phys. Rev. B* **1988**, *37*, 785; b) A. D. Becke, *J. Chem. Phys.* **1993**, *98*, 1372; c) A. D. Becke, *J. Chem. Phys.* **1993**, *98*, 5648.
[29] A. Schäfer, C. Huber, R. Ahlrichs, *J. Chem. Phys.* **1994**, *100*, 5829.
[30] A. Klamt, G. Schüürmann, *J. Chem. Soc. Perkin Trans. 2* **1993**, 799.

Received: February 20, 2013
Published Online: May 31, 2013

